Electrical and ultraviolet characterization of 4H-SiC Schottky photodiodes

Article (Published Version)

Electrical and ultraviolet characterization of 4H-SiC Schottky photodiodes

G. Lioliou,[1,*] M.C. Mazzillo,[2] A. Sciuto,[3] and A.M. Barnett[1]

[1]*Dept. Engineering and Design, Sch. of Engineering and Informatics, University of Sussex, Falmer, Brighton, BN1 9QT, UK*

[2]*Research and Development, Industrial and Power Discrete Group, (IPD R&D) STMicroelectronics, Catania 95121, Italy*

[3]*National Research Council, Institute for Microelectronics and Microsystems, (CNR-IMM) Catania 95121, Italy*

[*]*G.Lioliou@sussex.ac.uk*

Abstract: Fabrication and electrical and optical characterization of 4H-SiC Schottky UV photodetectors with nickel silicide interdigitated contacts is reported. Dark capacitance and current measurements as a function of applied voltage over the temperature range 20 °C – 120 °C are presented. The results show consistent performance among devices. Their leakage current density, at the highest investigated temperature (120 °C), is in the range of nA/cm^2 at high internal electric field. Properties such as barrier height and ideality factor are also computed as a function of temperature. The responsivities of the diodes as functions of applied voltage were measured using a UV spectrophotometer in the wavelength range 200 nm - 380 nm and compared with theoretically calculated values. The devices had a mean peak responsivity of 0.093 A/W at 270 nm and −15 V reverse bias.

OCIS codes: (250.0040) Detectors; (040.5160) Photodetectors; (160.6000) Semiconductor materials; (260.7190) Ultraviolet; (120.6780) Temperature.

References and links

1. E. Monroy, F. Omnès, and F. Calle, "Wide-bandgap semiconductor ultraviolet photodetectors," Semicond. Sci. Technol. **18**(4), R33–R51 (2003).
2. M. Razeghi and A. Rogalski, "Semiconductor ultraviolet detectors," J. Appl. Phys. **79**(10), 7433–7473 (1996).
3. D. Prasai, W. John, L. Weixelbaum, O. Krüger, G. Wagner, P. Sperfeld, S. Nowy, D. Friedrich, S. Winter, and T. Weiss, "Highly reliable silicon carbide photodiodes for visible-blind ultraviolet detector applications," J. Mater. Res. **28**(01), 33–37 (2013).
4. R. J. Drost and B. M. Sadler, "Survey of ultraviolet non-line-of-sight communications," Semicond. Sci. Technol. **29**(8), 084006 (2014).
5. X. Chen, H. Zhu, J. Cai, and Z. Wu, "High-performance 4H-SiC-based ultraviolet p-i-n photodetector," J. Appl. Phys. **102**(2), 024505 (2007).
6. A. Sciuto, F. Roccaforte, S. Di Franco, V. Raineri, and G. Bonanno, "High responsivity 4H-SiC Schottky UV photodiodes based on the pinch-off surface effect," Appl. Phys. Lett. **89**(8), 081111 (2006).
7. J. A. Angelo, *Spacecraft for Astronomy* (Infobase 2007).
8. F. Yan, X. Xin, S. Aslam, Y. Zhao, D. Franz, J. H. Zhao, and M. Weiner, "4H-SiC UV photo detectors with large area and very high specific detectivity," IEEE J. Quantum Electron. **40**(9), 1315–1320 (2004).
9. J. L. Barth, C. S. Dyer, and E. G. Stassinopoulos, "Space, atmospheric, and terrestrial radiation environments," IEEE Trans. Nucl. Sci. **50**(3), 466–482 (2003).
10. X. Chen, W. Yang, and Z. Wu, "Visible blind p-i-n ultraviolet photodetector fabricated on 4H-SiC," Microelectron. Eng. **83**(1), 104–106 (2006).
11. J. Cai, X. Chen, R. Hong, W. Yang, and Z. Wu, "High-performance 4H-SiC-based p-i-n ultraviolet photodiode and investigation of its capacitance characteristics," Opt. Commun. **333**(0), 182–186 (2014).
12. J. Hu, X. Xin, J. H. Zhao, F. Yan, B. Guan, J. Seely, and B. Kjornrattanawanich, "Highly sensitive visible-blind extreme ultraviolet Ni/4H-SiC Schottky photodiodes with large detection area," Opt. Lett. **31**(11), 1591–1593 (2006).
13. N. Watanabe, T. Kimoto, and J. Suda, "4H-SiC pn photodiodes with temperature-independent photoresponse up to 300 °C," Appl. Phys. Express **5**(9), 094101 (2012).

#236962 Received 26 Mar 2015; revised 29 May 2015; accepted 22 Jun 2015; published 11 Aug 2015

14. M. Mazzillo, G. Condorelli, M. E. Castagna, G. Catania, A. Sciuto, F. Roccaforte, and V. Raineri, "Highly efficient low reverse biased 4H-SiC Schottky photodiodes for UV-light detection," IEEE Photon. Technol. Lett. **21**(23), 1782–1784 (2009).
15. M. Mazzillo, A. Sciuto, F. Roccaforte, and V. Raineri, "4H-SiC Schottky photodiodes for ultraviolet light detection," in *IEEE Nuclear Science Symposium and Medical Imaging Conference*, (2011), pp. 1642–1646.
16. M. Mazzillo, A. Sciuto, G. Catania, F. Roccaforte, and V. Raineri, "Temperature and light induced effects on the capacitance of 4H-SiC Schottky photodiodes," IEEE Sens. J. **12**(5), 1127–1130 (2012).
17. G. Adamo, D. Agro, S. Stivala, A. Parisi, L. Curcio, A. Ando, A. Tomasino, C. Giaconia, A. C. Busacca, M. C. Mazzillo, D. Sanfilippo, and G. Fallica, "Responsivity measurements of silicon carbide Schottky photodiodes in the UV range," in *Third Mediterranean Photonics Conference*, (IEEE, 2014), pp. 1–3
18. G. Gramberg, "Temperature dependence of space charge capacitance of silicon carbide diodes," Solid-State Electron. **14**(11), 1067–1070 (1971).
19. S. M. Sze, *Physics of Semiconductor Devices*. (John Wiley & Sons 1981).
20. S. K. Cheung and N. W. Cheung, "Extraction of Schottky diode parameters from forward current-voltage characteristics," Appl. Phys. Lett. **49**(2), 85–87 (1986).
21. F. Roccaforte, F. La Via, V. Raineri, R. Pierobon, and E. Zanoni, "Richardson's constant in inhomogeneous silicon carbide Schottky contacts," J. Appl. Phys. **93**(11), 9137–9144 (2003).
22. R. T. Tung, "Electron transport of inhomogeneous Schottky barriers," Appl. Phys. Lett. **58**(24), 2821–2823 (1991).
23. G. Bertuccio, S. Caccia, D. Puglisi, and D. Macera, "Advances in silicon carbide X-ray detectors," Nucl. Instrum. Methods Phys. Res. A **652**(1), 193–196 (2011).
24. J. A. Kittl, M. A. Pawlak, A. Lauwers, C. Demeurisse, K. Opsomer, K. G. Anil, C. Vrancken, M. J. H. van Dal, A. Veloso, S. Kubicek, P. Absil, K. Maex, and S. Biesemans, "Work function of Ni Silicide phases on HfSiON and SiO_2: NiSi, Ni_2Si, $Ni_{31}Si_{12}$, and Ni_3Si fully silicided gates," IEEE Electron Device Lett. **27**(1), 34–36 (2006).
25. F. Roccaforte, F. La Via, A. La Magna, S. Di Franco, and V. Raineri, "Silicon carbide pinch rectifiers using a dual-metal Ti-Ni_2Si Schottky barrier," IEEE Trans. Electron. Dev. **50**(8), 1741–1747 (2003).
26. Anon, "Broadband SiC based UV photodiode A = 0.50 mm^2, SG01D–18," Rev.6.0, SGlux SolGel Technologies GmbH, Berlin, Germany. N.D.
27. Anon, "Broadband SiC based UV photodiode A = 1.00 mm^2, SG01L–18," Rev.6.0, SGlux SolGel Technologies GmbH, Berlin, Germany. N.D.
28. S. G. Sridhara, R. P. Devaty, and W. J. Choyke, "Absorption coefficient of 4H silicon carbide from 3900 to 3250 Å," J. Appl. Phys. **84**(5), 2963–2964 (1998).
29. G. Brezeanu, F. Udrea, A. Mihaila, G. Amaratunga, J. Millan, P. Godignon, M. Badila, F. Draghici, C. Boianceanu, and M. Brezeanu, "Numerical and analytical study of 6H-SiC detectors with high UV performance," in *Proceedings of Semiconductor Conference*, (2002), pp. 185–188.
30. K. S. Park, "High quantum-efficiency 4H-SiC UV photodiode," J. Korean Phys. Soc. **30**(1), 123–130 (1997).
31. H. Y. Cha and P. M. Sandvik, "Electrical and optical modeling of 4H-SiC avalanche photodiodes," Jpn. J. Appl. Phys. **47**(7), 5423–5425 (2008).
32. A. Sciuto, M. Mazzillo, P. Badala, M. Scuderi, B. Carbone, and S. Coffa, "Thin metal film Ni2Si/4H-SiC vertical Schottky photodiodes," IEEE Photon. Technol. Lett. **26**(17), 1782–1785 (2014).

1. Introduction

Ultraviolet (UV) photodetectors are used in a wide range of applications. Civil applications include food, air and drinking water purification, chemical and biological analysis, industrial flame detection as well as UV sterilization of medical equipment [1–3]. They are also employed in areas such as security, dermatology and inter-satellite and non-line-of-sight communications [1,4–6], with military applications including missile warning, missile plume sensing and combustion monitoring [1,5]. UV data gathered using high altitude balloons, rocket probes and space telescopes can also be very useful in investigating astronomical phenomena [7].

Semiconductor detectors made from materials with narrow bandgaps (such as silicon), can face limitations when used for UV detection due to their material properties. For instance, when operated in high temperature environments (>> 20 °C) such photodetectors must often be cooled to reduce their leakage current and consequently the noise of the system [3,8]. This cooling not only increases the mass, power consumption and cost of the system but can also degrade the detectivity of the cooled device if it behaves as a cold trap for contaminants [1]. Additionally, radiation of much higher energy than the bandgap energy can cause device aging and failure [1,3]. The background radiation, which is mainly in the visible

#236962 Received 26 Mar 2015; revised 29 May 2015; accepted 22 Jun 2015; published 11 Aug 2015

and infrared for terrestrial applications, can also introduce noise due to these photons also being detectable when their energy is greater than the band gap [8].

However, UV detectors based on wide bandgap semiconductor materials, such as SiC, can overcome many of those issues. Due to their larger bandgaps, devices based on such materials can have dark currents orders of magnitude lower than silicon photodetectors of comparable design [3, 5], and hence, they can operate at room temperature and above without cooling. Another advantage of SiC, for UV applications, is the intrinsic insensitivity (visible-blindness) to photons of energy < 3.2 eV (wavelength 380 nm). Consequently, SiC UV photodiodes can operate even in high flux visible and IR backgrounds without the use of filters [8]. A further benefit comes from the strong bonding in SiC which increases device radiation hardness [3]; as such, SiC suffers less from device aging due to radiation damage [1] and consequently SiC detectors can have much longer lifetimes in intense energetic radiation applications, as would be required for space missions to intense radiation environments such as Jupiter and its moons [9] and the inner solar system. As a result, UV detectors made from SiC are potentially highly attractive devices and worthy of detailed study.

A variety of device structures have been reported for the development of high-performance 4H-SiC UV photodiodes in the past. The first 4H-SiC p-i-n photodetectors presented in [10], in which photocurrent measurements under UV illumination as a function of applied reverse bias were reported. More recently, electrical characterization and photoresponsivity measurements on 4H-SiC p-i-n photodetectors were reported in [11], showing a leakage current density of 9.95×10^{-8} A/cm^2 at 100 kV/cm internal electric field, and a peak responsivity of 0.15 A/W at 268 nm, both at 450 K temperature. In [12], Hu et al. reported Ni/4H-SiC Schottky photodiodes showing a leakage current density of 0.4×10^{-12} A/cm^2 at 8 kV/cm internal electric field, at room temperature and a peak quantum efficiency of 65% at 276 nm, at photovoltaic mode operation. 4H-SiC Schottky photodiodes of different sizes were reported in [8], having a leakage current density of 8×10^{-11} A/cm^2 at 13.5 kV/cm internal electric field, at room temperature and a nearly flat quantum efficiency from 240 nm to 320 nm of over 30%. Photoresponsivity measurements on 4H-SiC p-n photodiodes were reported in [13], at temperatures up to 300 °C, showing temperature independent response at a wavelength which depended on the applied reverse bias.

In this paper we report electrical and optical characterization of 4H-SiC Schottky UV detectors with nickel silicide (Ni_2Si) interdigitated contacts. The interdigitated contacts allow the active region of the devices to be directly exposed to the UV radiation, enabling high quantum efficiency. 4H-SiC Schottky diodes employing the same nickel silicide interdigit structures have been reported in [6,14–17]. However, the devices reported here have the thickest epilayer. Also, a direct comparison between four randomly selected diodes is done. Moreover, an extensive electrical characterization including forward and reverse bias capacitance and dark current measurements are reported at temperatures up to 120 °C, the highest reported temperature for similar devices. All the devices showed consistent capacitances and very low leakage current even at the maximum investigated internal electric field (= 83 kV/cm). Responsivity measurements as a function of wavelength and applied bias are also reported and examined.

2. Device structure and fabrication

The Schottky photodiodes were fabricated in STMicroelectronics-Catania R&D facilities on-type 4H-SiC epitaxial layers, 6 μm thick, grown by CREE Inc., onto an n-type heavily doped substrate. The doping concentration of the substrate was 10^{19} cm^{-3}, with the dopant being nitrogen, and the doping concentration of the epilayer was 10^{14} cm^{-3}, as indicated by the supplier. Ohmic contacts on the sample back side were formed by sputtering of a 200 nm Ni film, followed by a rapid annealing at 1000 °C. Schottky contacts on the device front were

#236962 Received 26 Mar 2015; revised 29 May 2015; accepted 22 Jun 2015; published 11 Aug 2015

obtained by defining Ni_2Si interdigit structures. The definition of 3 μm wide Ni_2Si stripes was obtained by combining standard optical lithography and highly selective metal etch. The pitch of the Ni_2Si stripes was 10 μm. A rapid thermal processing at 700 °C was used for the treatment of the front Schottky barrier [6]. A 1 μm thick AlSiCu metal layer was sputtered on the top side of the device defining the anode contact pad and a metallic multilayer Ti-Ni-Au (1 kÅ/5 kÅ/0.5 kÅ) was sputtered on the rear of the wafer defining the cathode ohmic contact. In Fig. 1, a simplified not to scale schematic of the device and an optical microscopy top view image are reported: photodiodes have square geometry, total area of 1.2 × 1.2 mm^2 and a 4H-SiC area of about 1 mm^2 directly exposed to the radiation (70% of fill factor). The photodiodes were packaged in TO-18 cans with a suitable UV light transparent quartz window.

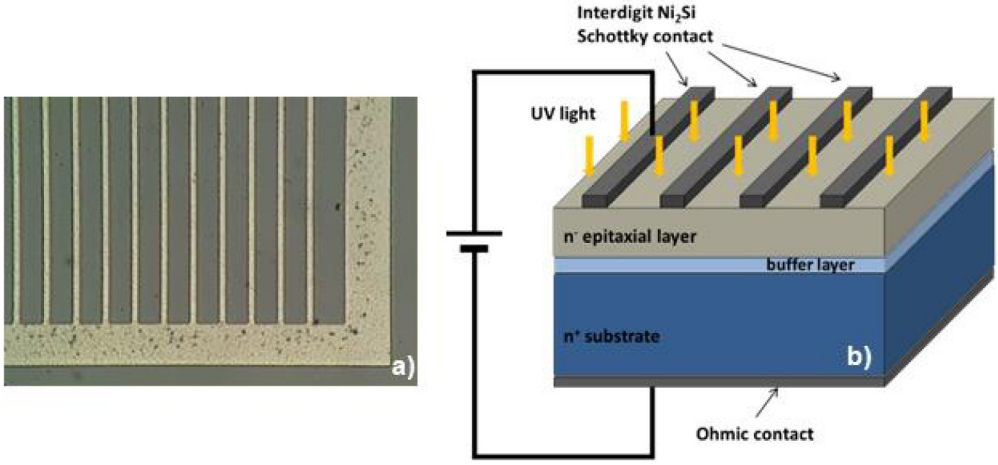

Fig. 1. 4H-SiC Schottky photodiode (a) layout top view and (b) a schematic side drawing.

3. Experimental results

3.1. Electrical characterization

3.1.1. Capacitance–voltage measurements

To determine the effective doping density and compute the depletion width of the devices, the devices' capacitances were investigated as functions of applied forward and reverse bias and temperature (120 °C to 20 °C),using an HP 4275A Multi Frequency LCR meter, and a TAS Micro MT climatic cabinet. The test signal was sinusoidal with a 50 mV rms magnitude and 1 MHz frequency. Capacitance measurements were made at reverse voltages between 0 V and −50 V and at forward voltages between 0 V and + 1 V. The capacitance of the package was determined by measuring empty packages; the packaging capacitance was found to be 0.61 pF ± 0.02 pF (rms deviance). Figure 2 shows the reverse and forward bias *C–V* characteristics of the four photodiodes (packaging capacitances subtracted) when measured at 20 °C, and Fig. 3 shows the reverse and forward bias *C–V* characteristics as a function of temperature for one representative device, diode D3.

#236962 Received 26 Mar 2015; revised 29 May 2015; accepted 22 Jun 2015; published 11 Aug 2015

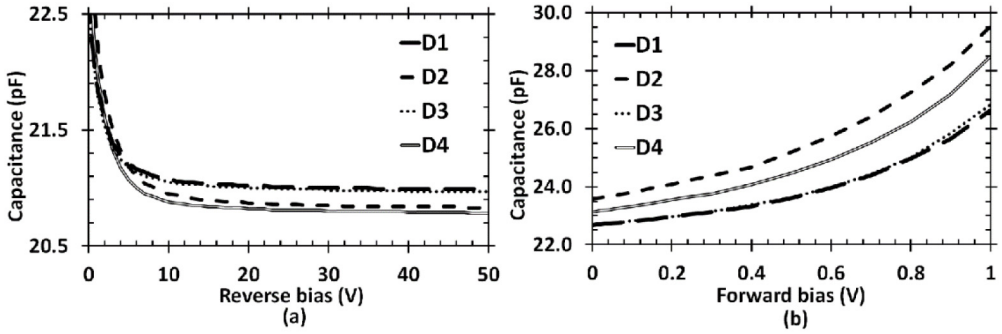

Fig. 2. Capacitance – Voltage characteristics measured at a temperature of 20 °C for the four 4H-SiC Schottky photodiodes, D1 – D4, as a function of (a) reverse and (b) forward bias.

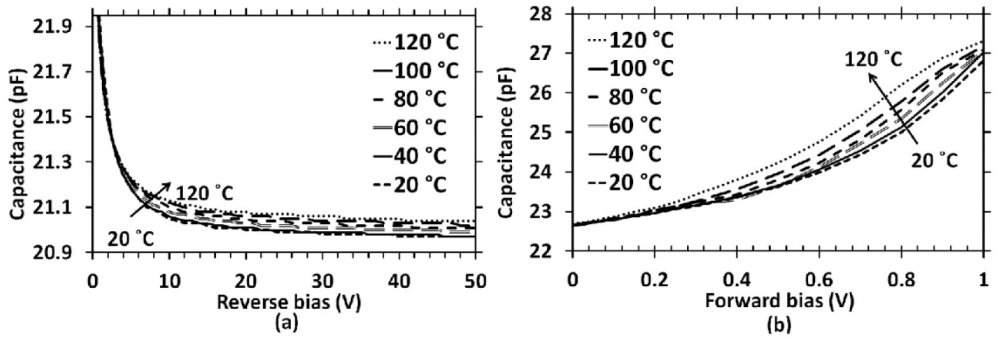

Fig. 3. Forward (a) and reverse (b) Capacitance – Voltage measurements as a function of temperature (20 °C - 120 °C) for a representative diode (D3).

At 20 °C, as the reverse bias was increased in magnitude from 0 V to −5 V the capacitance of the diodes decreased by a mean value of 1.85 pF. Increasing the reverse bias further resulted in only a small additional decrease in capacitance: there was a mean additional reduction of 0.17 pF in capacitance as the reverse bias was increased from −5 V to −10 V, and an average 0.10 pF reduction as the reverse bias was further increased from −10 V to −50 V. The small decrease in capacitance at reverse biases beyond −10V indicates that the epitaxial layer is almost fully depleted at this voltage. At each applied reverse bias, the capacitance increased as the temperature increased. This may be attributed to the increasing effective charge density in the space charge region with temperature; similar effects have been explained by the presence of deep level defects and the carriers trapped by them [11,16,18].

The depletion width, W, of the photodiodes was computed as per the one-sided abrupt p^+ - n junction,

$$W = \frac{A\varepsilon_s}{C} \tag{1}$$

where A is the area of the photodiode. ε_s is the permittivity, and C is the measured capacitance [19]. At 20 °C, the depletion width for a representative device (D4) was computed to be 5.3 μm when biased at 0 V. When the reverse voltage was −5 V, the depletion width increased to 5.8 μm. At −10 V, the depletion width increased to 5.9 μm. At the largest reverse bias investigated (−50 V), the depletion width was determined to be 5.9 μm.

#236962 Received 26 Mar 2015; revised 29 May 2015; accepted 22 Jun 2015; published 11 Aug 2015

The effective doping density, N_{eff}, was determined by plotting $1/C^2$ as a function of applied bias V (as per [19]), such that N_{eff} was given by

$$N_{eff} = \frac{2}{q\varepsilon_s A^2 \dfrac{d\left(1/C^2\right)}{dV}} \tag{2}$$

where q is the charge on an electron, and all other symbols have been previously defined.

Figure 4 shows the effective doping density, N_{eff}, for a representative diode (D4) determined from $d(1/C_2)/dV$ at 120 °C and 20 °C. At 50 V, the mean maximum thickness of the depletion layer for all four photodiodes was calculated to be 5.9 μm at both 20 °C and 120 °C. At 20 °C, the doping concentration was consequently determined to vary from (6.27 ± 0.29) × 10^{13} cm^{-3} at the Schottky contact to (3.24 ± 0.04) × 10^{16} cm^{-3} at the interface between the n epilayer and the substrate. Similarly, at 120 °C, the doping concentration was determined to vary from (1.58 ± 0.11) × 10^{14} cm^{-3} at the Schottky contact to (3.26 ± 0.03) × 10^{16} cm^{-3} at the interface between the n epilayer and the substrate. The doping profile of the devices, as is shown in Fig. 4, follows an exponential trend, rather than an abrupt change between the epilayer and substrate.

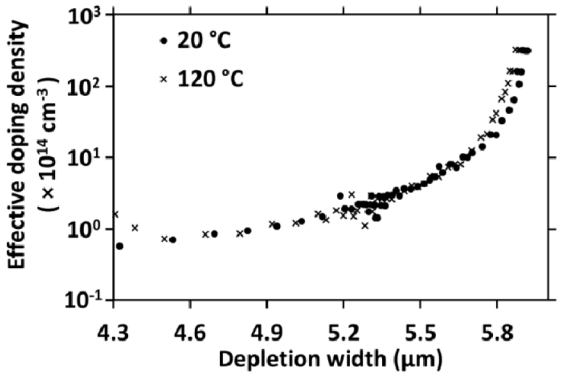

Fig. 4. The effective doping density for a representative diode as determined by Capacitance-Voltage measurements at 20 °C (filled circles) and 120 °C (× symbol).

3.1.2. Current-voltage measurements

Both forward biased and reverse biased dark current measurements as a function of applied voltage (*I-V* characteristics) of all four photodiodes were measured at temperatures of 20 °C to 120 °C using a Keithley 6487 Picoammeter/Voltage Source and a TAS Micro MT climatic cabinet. Figure 5 shows the forward $I - V$ characteristics of all four photodiodes. The forward bias Current – Voltage characteristics as a function of temperature of a representative diode, D4, are presented in Fig. 6.

#236962 Received 26 Mar 2015; revised 29 May 2015; accepted 22 Jun 2015; published 11 Aug 2015

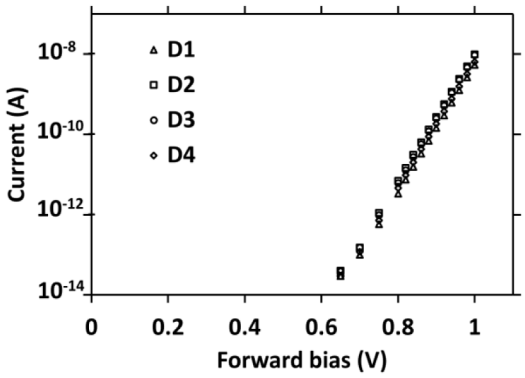

Fig. 5. Current as a function of applied forward bias at a temperature of 20 °C for the four 4H-SiC Schottky photodiodes (D1 – D4).

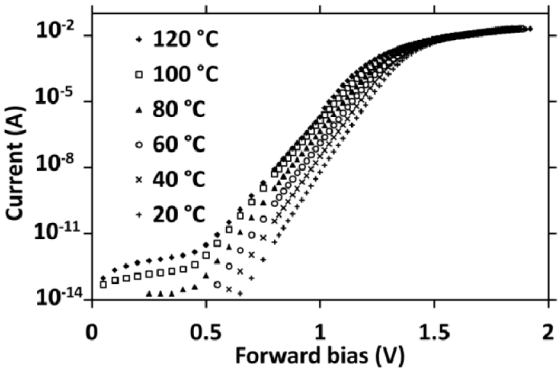

Fig. 6. Forward *I – V* characteristics measured for diode D4 in the temperature range 20 °C – 120 °C.

Two parameters of a Schottky diode, the ideality factor, n, and the barrier height, φ_B, were extracted from the forward $I-V$ measurements following the Cheung method [20]. The ideality factor, n, was computed from the intercept point of the $d(V)/d(lnI) - I$ graph. The barrier high, φ_B, was obtained from the equation:

$$\phi_B = \frac{kT}{q} ln\left(\frac{SA^*T^2}{I_s}\right) \tag{3}$$

where S is the photodiode's area, $A^* = 146$ A K^{-2} cm^{-2} is the effective Richardson constant and I_s is the saturation current [19]. The saturation current, I_s, was found from extrapolating the linear region of the forward $I - V$ curves at zero voltage. As an example, the saturation current, I_s, for D2 was found to be 19.8×10^{-25}A $\pm$ 1.1×10^{-25}A at 20 °C from a single forward *I-V* plot and linear least squares fitting, taking into account the standard deviation of the intercept point and combination of errors. The mean saturation current, I_s, of all four photodiodes, calculated using the same procedure, was $(12.5 \pm 8.7) \times 10^{-25}$A at 20 °C.

The computed barrier height and ideality factor of D4, as a function of temperature can be seen in Fig. 7.

#236962 Received 26 Mar 2015; revised 29 May 2015; accepted 22 Jun 2015; published 11 Aug 2015

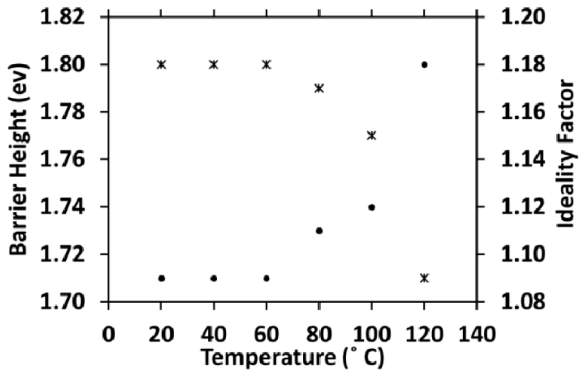

Fig. 7. Barrier height (filled circles) and ideality factor (stars) extracted from forward current – voltage measurements using the Cheung method in the temperature range 20 °C – 120 °C for D4.

The ideality factor, n, improved from 1.18 at 20 °C to 1.09 at 120 °C and the barrier height, φ_B, increased from 1.71 eV at 20 °C to 1.80 eV at 120 °C. As temperature decreased, there was a bigger deviation from the ideal, with the barrier height to appearing to be lowered. This observation suggested the presence of an inhomogeneous barrier [21]. In [22], Tung showed that the current through an inhomogeneous Schottky barrier may be expressed as the sum of currents flowing in an assortment of Schottky barrier height (SBH) patches that are low. More specifically, Tung provided an analytical form of the current flowing to and from a small SBH low patch which can explain these widely reported, abnormal experimental results. Current transport across the metal-semiconductor interface at low temperatures is dominated by electrons surmounting the lower barriers, resulting in a larger ideality factor and in a lower apparent Schottky barrier height. However, as temperature increases, electrons have more energy to overcome higher barriers, resulting in an increase of the dominant barrier height. Tung's theory shows that the observed change in ideality factor and barrier height with temperature is a natural result of an inhomogeneous SBH. The improvement of the ideality factor and the increment of the barrier height as the temperature increased, of the currently reported photodiodes can be similarly explained.

The reverse $I - V$ characteristics of all four 4H-SiC Schottky photodiodes measured at 20 °C are shown in Fig. 8. It should be noted that due to the devices' thin epilayers (~6 μm), applied reverse biases of −50 V create a mean electric field of 83 kV/cm across the depletion region. However, even at this field strength (83 kV/cm), the leakage current at 20 °C remained ≤ 0.2×10^{-12} A (13×10^{-12} A /cm^2) for three of the tested devices (D2 – D4), with D1 showing a leakage current of 2.5×10^{-12} A (173×10^{-12} A /cm^2). For a representative device from the set of three diodes that showed the lowest leakage currents, I-V characteristics as a function of temperature are shown in Fig. 9. The leakage current densities in the detectors we report are lower compared to previously reported for similar devices (similar n^- epilayer thickness) at low reverse bias e.g. in [14], Mazzillo et al reported 242×10^{-12} A /cm^2 current density at −5 V, whereas the currently reported devices e.g. D4 has a current density of 187×10^{-12} A /cm^2 at −5 V reverse applied bias at 100 °C.

#236962 Received 26 Mar 2015; revised 29 May 2015; accepted 22 Jun 2015; published 11 Aug 2015

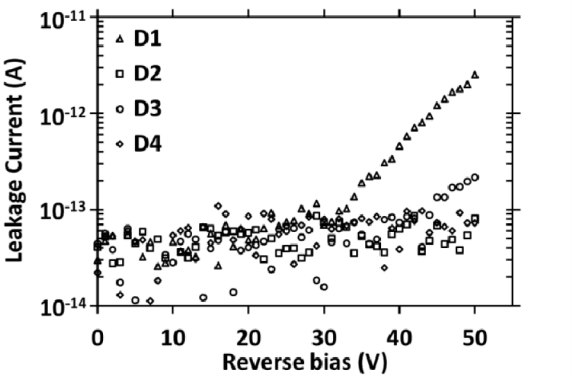

Fig. 8. Measured leakage current as a function of applied reverse bias for the four 4H-SiC Schottky photodiodes, when measured at a temperature of 20 °C.

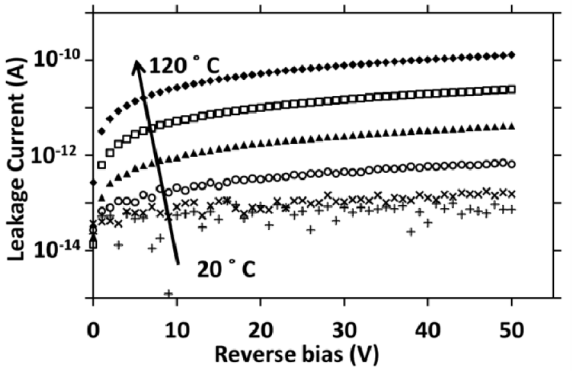

Fig. 9. Measured leakage current as a function of applied reverse bias for a representative 4H-SiC Schottky photodiode, D4, in the temperature range 20 °C - 120 °C.

The measured current density of a representative device, D4, as a function of temperature at three internal electric fields is shown in Fig. 10. At the highest investigated temperature (120 °C), the current density is still low (in the range of 10^{-9} A /cm^2) despite the internal electric field being up to 83 kV/cm (see Fig. 10). These leakage current densities are comparable with those reported for other high quality 4H-SiC Schottky devices (e.g. 1×10^{-9} A /cm^2 at 100 °C at a mean internal electric field of 103 kV/cm [23]). Although the current density follows a clearly exponential increase as temperature increases from 40 °C to 120 °C, due to more thermally generated carriers as the temperature increases, the measurement system limits the current measurements at lower temperatures.

Such low leakage current densities can be attributed to high material quality. The Schottky (rectifying) contact can also have an effect on the leakage current of the devices. The barrier height of the Ni_2Si/4H-SiC Schottky contact was measured to be 1.71 eV at 20 °C and 1.80 eV at 120 °C. These high values resulted from the work function of Ni_2Si being ~4.8 eV [24]. Since the leakage current of a Schottky diode arises from the majority carriers (in this case e^-) at the metal side overcoming the barrier height, the apparent low leakage current may be related to the high barrier height formed from the Ni_2Si/4H-SiC contact. Similar explanation was given in [25], where Ni_2Si/4H-SiC Schottky diodes had a higher barrier height and significantly lower leakage current than Ti/4H-SiC Schottky diodes.

#236962 Received 26 Mar 2015; revised 29 May 2015; accepted 22 Jun 2015; published 11 Aug 2015

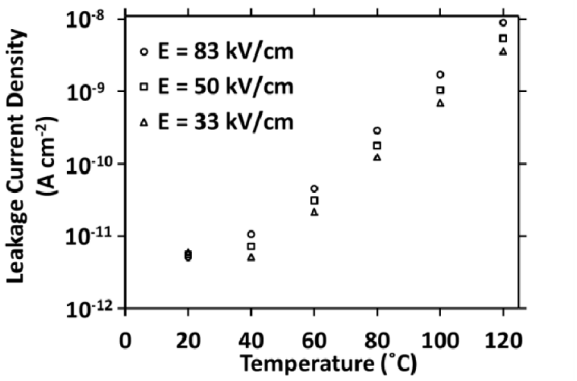

Fig. 10. Measured current density of a SiC Schottky photodiode as a function of temperature at three electric fields.

3.2. UV characterization

To investigate the performance of the detectors under UV illumination, responsivity measurements were made using a ThermoSpectronic UV300 UV-VIS spectrophotometer with Tungsten, Deuterium and Mercury lamps to cover the wavelength range 210 nm to 500 nm. The selection of the wavelength of interest was performed using an internal monochromator and UV grating. Two SG Lux SiC photodetectors with different areas and known responsivities [26,27] were used as reference photodiodes to calibrate the apparatus. The incident UV power illuminating the devices was small (less than 2 nW) in the investigated wavelength range of 210 nm – 500 nm, while the photocurrent measured with the devices reported here was from ~1 pA to ~100 pA. Custom baffles were used in order to ensure that no external sources of light could influence the measurements.

UV responsivity spectra of the four devices are shown in Fig. 11 as a function of the incident photons' wavelengths measured at room temperature and in photovoltaic operation condition (i.e. reverse bias = 0 V). A responsivity peak value of 0.037 A/W ± 0.007 A/W (QE = 16%, using Eq. (7)) was measured at 280 nm at room temperature when no reverse bias was applied for all four photodiodes. The responsivity did not have an abrupt spectral cutoff since 4H-SiC is indirect semiconductor and does not have a sharp cutoff band edge [5]. The absorption coefficient, α, is inversely proportional to wavelength and, in part, determines the quantum efficiency [19]. It increases from 380 nm (= 3.23 eV = E_g) to shorter wavelengths and as a result, the responsivity follows the same trend [28]. The responsivity slowly increased from 380 nm (= 3.23 eV = E_g) to shorter wavelengths, as the absorption coefficient, α, increased [28]. The penetration depth, $1/\alpha$, at 380 nm was much larger (~625 μm) than the width of the space charge region of the devices (~6 μm) [5]. Hence, most of the incident photons penetrated through the active region resulting in low photocurrent. As the wavelength became shorter, the penetration depth decreased and more photons were absorbed and generated electron-hole pairs in the detector. The maximum photoresponsivity was achieved at around 280 nm, with shorter wavelengths showing decreased photoresponsivity. This may be attributed to the fact that for $\lambda < 280$ nm the penetration length (< 1 μm [5]) becomes comparable with the dead zone introduced by the surface recombination resulting in the generated carriers recombining and not contributing to the photoresponse [5].

#236962 Received 26 Mar 2015; revised 29 May 2015; accepted 22 Jun 2015; published 11 Aug 2015

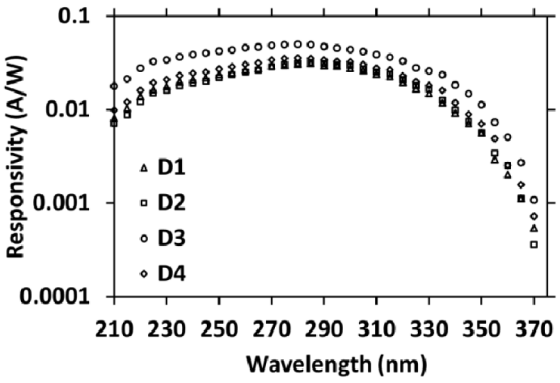

Fig. 11. Responsivity as a function of wavelength (210 nm to 380 nm) measured for each 4H-SiC Schottky photodiode, D1 – D4, at room temperature when biased at 0 V.

The theoretical responsivity, R_{Th}, as a function of wavelength, was computed and compared with the measured responsivity, R. The internal quantum efficiency, QE_{int}, defined as the probability that an incoming photon is absorbed in the active area of the device [15], was calculated as a function of wavelength by,

$$QE_{int} = \left(1 - \frac{e^{-\alpha W}}{1 + \alpha L_p}\right) \tag{4}$$

where α is the absorption coefficient as a function of wavelength, W is the depletion layer width and L_p is the hole diffusion length [29]. The external quantum efficiency, QE, which is the average number of electron-hole pairs generated per incident photon [19], was computed using the following equation:

$$QE = T \times f_{geo} \times QE_{int} \tag{5}$$

where f_{geo} is the geometrical fill factor which equals the 4H-SiC area directly exposed to the radiation (= 70% for these devices) and T is the power transmission coefficient (as a function of wavelength) at the air-photodiode interface given by [15]:

$$T = \frac{4 n_{\mathrm{SiC}} n_0}{\left(n_{\mathrm{SiC}} + n_0\right)^2} \tag{6}$$

where n_{SiC} and n_0 are the refractive indices of SiC and air, respectively. Using the refractive index reported in [30] for 4H-SiC (= 3 at 270 nm and 2.6 at 280 nm), the absorption coefficient, α, reported in [31] for 4H-SiC (= 17000 cm^{-1} at 270 nm and 8000 cm^{-1} at 280 nm), the hole diffusion length L_p = 2 μm [5] and the depletion layer width, W, found from the capacitance-voltage measurements as a function of reverse bias, QE was calculated.

Once the QE was computed as a function of wavelength, the theoretical responsivity R_{Th} was found from the relationship,

$$QE = R \times 1.24 / \lambda \tag{7}$$

The factor $1.24/\lambda$ (= hc/λ, where h is the Planck constant and c is the speed of light) corresponds to photon energy (in eV) of wavelength λ (in μm) [19]. The theoretical value of the maximum R_{Th} (occurred at 280 nm) was constant between 0 V and −15 V (reverse) applied voltage, and equal to 0.12 A/W. Figure 12 shows a comparison between the measured and theoretical photoresponsivity at 280 nm as a function of applied voltage.

#236962 Received 26 Mar 2015; revised 29 May 2015; accepted 22 Jun 2015; published 11 Aug 2015

Figure 13 shows photoresponsivity spectra for a representative device, D2, with the applied reverse bias as parameter. The peak responsivity at 0 V and −5 V reverse bias occurred at 280 nm whereas the responsivity showed a peak value at 270 nm when the diode was reverse biased at −10 V and −15 V.

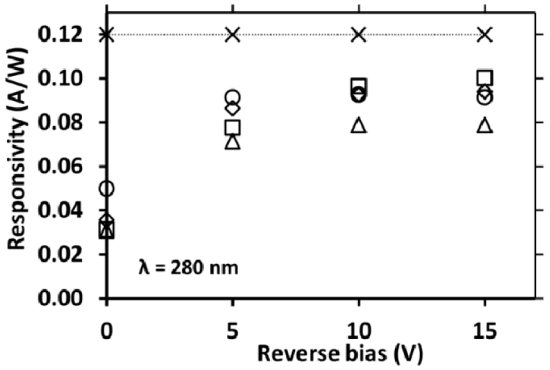

Fig. 12. Theoretical (crosses) and measured photoresponsivity for D1 (open triangles), D2 (open squares), D3 (open circles) and D4 (open diamonds) as a function of applied reverse bias, at room temperature.

Although the theoretical responsivity at 280 nm was 0.12 A/W for all investigated biases, the measured responsivity was well below this value for unbiased devices and increased with applied voltage. It increased considerably when the photodiodes were reverse biased at −5 V compared to 0 V. There is a further improvement in photoresponsivity at −10 V, but the responsivity increase at biases beyond this (−15 V) was comparatively small. The difference between the theoretical and measured responsivities at 280 nm and 0 V may be attributed to charge trapping and losses present in the active region of the device. As the internal field increased with increased reverse bias, the improved charge transport resulted in less trapping and less charge loss, with the consequence of more charge being induced on the contacts. At −15 V reverse bias, the measured photoresponsivity was much closer to the computed value, consistent with reduced charge transport losses at higher fields.

As the reverse biased increased in magnitude, the depletion layer width also increased. Hence, a red-shift (towards longer wavelengths) of the responsivity was expected (enhanced absorption of the long-wavelength photons) with increased bias. However, a red-shift was not observed. This was attributed to the small change of the depletion layer width as the reverse bias increased from 0 V (W_{0V} = 5.2 μm) to −15 V (W_{15V} = 5.9 μm). The peak of the theoretical responsivity was also computed to be invariant with this change in depletion layer width. A blue-shift of the responsivity peak was observed instead, with increased reverse bias. The improved charge transport with increased reverse bias might enhance the collection of charge carriers generated close to the surface (short-wavelength photons), which explains the blue-shift of the responsivity peak.

#236962 Received 26 Mar 2015; revised 29 May 2015; accepted 22 Jun 2015; published 11 Aug 2015

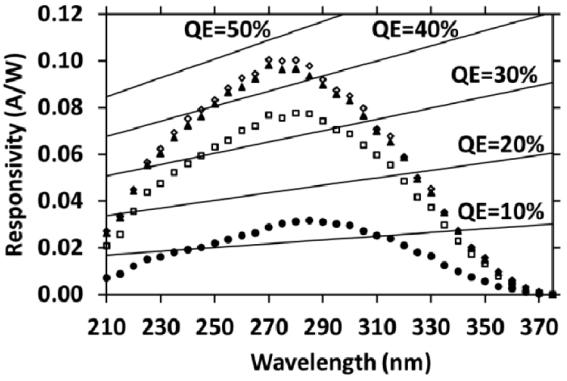

Fig. 13. Photoresponsivity spectra measured with representative diode D2 at room temperatureat reverse biases of 0 V (filled circles); 5 V (open squares); 10 V (filled triangles) and 15 V (open diamonds).

The photoresponsivity of diode D2 had a peak value of 0.100 A/W (QE = 46%, QE_{int} = 67.5%) at 270 nm when the device is reverse biased at −15 V. This value is comparable with previous reported results of similar devices [14,17]. The measured photoresponsivity at 270 nm and reverse bias of −15 V was 0.080 A/W, 0.098 A/W and 0.094 A/W for diode D1, D3 and D4 respectively.

The visible blindness, as defined by the peak responsivity in the UV range divided by the responsivity at 500 nm, was measured using a 500 nm light with a power of 105 pW. While irradiating a device with the 500 nm light, no photocurrent could be detected with the picoammeter (Keithley 6487) suggesting the photocurrent was <10 fA. When illuminating the four devices with the 270 nm light providing a power of 864 pW, a photocurrent of 81 pA ± 7 pA was measured. Due to the low power of the 500 nm light, only the maximum boundary of the UV–visible rejection ratio between the photoresponsivity at 500 nm and at 270 nm could be estimated. This ratio was found to be 10^{-3}. The real degree of visible blindness of the photodiode is expected to be better, as for previously reported similar devices [14,32].

4. Discussions, conclusions and further work

Four 4H-SiC Schottky UV detectors employing Ni_2Si interdigitated contacts have been characterized for their electrical and optical behaviour within the temperature range 20 °C to 120 °C. Forward and reverse biased capacitance (C-V) measurements showed consistent performance between the diodes. The depletion width and effective doping density calculations based on the capacitance measurements showed that the diodes were almost fully depleted at 10 V, due to the high quality of the epilayer. The devices' dark currents as functions of reverse and forward voltage and temperature were also measured. The devices' leakage current densities at room temperature, was found to be few pA/cm^2 (limited by the measuring system) and still < 10 nA/cm^2 at 120 °C at 83 kV/cm internal electric field.

UV photoresponsivity measurements at room temperature have been performed as a function of applied reverse voltage. The peak responsivity of all four detectors was at 280 nm, when operating in photovoltaic mode. Although the devices had modest responsivities (mean of 0.037 A/W ± 0.007 A/W) at 0 V applied reverse bias, the mean responsivity increased to 0.093 A/W ± 0.007 A/W when the detectors were reverse biased at −15 V. This was attributed to charge trapping and possibly recombination in the active region of the photodiodes at low internal electric fields. The dark leakage current for all photodiodes was measured to be < 70 fA at −15 V reverse bias at room temperature.

#236962 Received 26 Mar 2015; revised 29 May 2015; accepted 22 Jun 2015; published 11 Aug 2015

The internal quantum efficiency (as defined in section 3.2, Eq. (5)) of the detectors was measured to be 87.9% at 270 nm for the best performance device, with the detector reverse biased at −15 V. Also, the UV–visible rejection ratio (photoresponsivity at 500 nm divided by photoresponsivity at 270 nm) was measured to be at least 10^{-3}, although the true UV-visible rejection ratio is likely to be far better. The results reported here show that with low operation voltages, low leakage current densities and good UV responsivity (0.100 A/W peak responsivity, with at least 10^{-3} visible blindness) the detectors are promising devices for UV detection in applications such as space science and harsh terrestrial environments. Further work including UV responsivity measurements as a function of temperature is planned and will be reported separately in due course, as will measurements of the radiation hardness of the devices with a view to characterising their likely long term performance for space missions to intense radiation environments such as possible future exploration of the Jupiter and Saturn planetary systems, space weather monitoring and exploration of the inner solar system close to the Sun.

Acknowledgments

The authors gratefully acknowledge M. Henry and M. Osborne, Dept. of Chemistry, School of Life Sciences, University of Sussex, UK, for the use of the spectrophotometer. G. Lioliou acknowledges funding received from University of Sussex in the form of a PhD scholarship.

#236962 Received 26 Mar 2015; revised 29 May 2015; accepted 22 Jun 2015; published 11 Aug 2015